

# Chronic Lymphocytic Inflammation Specifies the Organ Tropism of Prions

Mathias Heikenwalder,<sup>1\*</sup> Nicolas Zeller,<sup>1\*</sup> Harald Seeger,<sup>1\*</sup> Marco Prinz,<sup>1\*†</sup> Peter-Christian Klöhn,<sup>2</sup> Petra Schwarz,<sup>1</sup> Nancy H. Ruddle,<sup>3</sup> Charles Weissmann,<sup>2</sup> Adriano Aguzzi<sup>1‡</sup>

Prions typically accumulate in nervous and lymphoid tissues. Because pro-inflammatory cytokines and immune cells are required for lymphoid prion replication, we tested whether inflammatory conditions affect prion pathogenesis. We administered prions to mice with five inflammatory diseases of the kidney, pancreas, or liver. In all cases, chronic lymphocytic inflammation enabled prion accumulation in otherwise prion-free organs. Inflammatory foci consistently correlated with lymphotoxin up-regulation and ectopic induction of FDC-M1<sup>+</sup> cells expressing the normal cellular prion protein PrP<sup>C</sup>. By contrast, inflamed organs of mice lacking lymphotoxin- $\alpha$  or its receptor did not accumulate the abnormal isoform PrP<sup>Sc</sup>, nor did they display infectivity upon prion inoculation. By expanding the tissue distribution of prions, chronic inflammatory conditions may act as modifiers of natural and iatrogenic prion transmission.

Prions, the infectious agent in transmissible spongiform encephalopathies that selectively damage the central nervous system (CNS), are detectable in lymphoid organs long before clinical symptoms appear (1). PrP<sup>Sc</sup>, a protease-resistant isoform of the host protein PrP<sup>C</sup>, accumulates mostly in the CNS and lymphoid organs of infected organisms and may represent the infectious principle (2, 3). In addition to PrP<sup>C</sup> (4), splenic prion replication requires follicular dendritic cells (FDCs) (5), whose maintenance depends on B cells expressing tumor necrosis factor (TNF) and lymphotoxins (LTs)  $\alpha$  and  $\beta$  (6–8). Accordingly, inhibition of LT and TNF antagonizes peripheral prion replication (9–11). However, most cellular requirements for peripheral prion replication remain unknown (12).

Chronic inflammatory conditions are accompanied by organized collections of B and T lymphocytes, FDCs, dendritic cells (DCs), and marginal zone and tingible body macrophages (13–15). Extranodal follicles are also prevalent in naturally occurring infections of free-ranging ruminants (16). Besides participating in chronic inflammatory conditions, FDCs, B lymphocytes, and

other components of the immune system are involved in prion replication (6–10, 17). We therefore reasoned that inflammation may affect prion pathogenesis. We studied this question in various transgenic and spontaneous mouse models of chronic inflammation, including nephritis, pancreatitis, and hepatitis.

First, we generated bitransgenic mice expressing LT $\alpha$  and LT $\beta$  in liver under the control of the albumin promoter (fig. S1A) (18, 19). C57BL/6-Tg(LTab)1222 and C57BL/6-Tg(LTab)1223 mouse lines contained one copy per haploid genome of both AlbLT $\alpha$  and AlbLT $\beta$  transgenes (fig. S1B), with expression restricted to liver and absent from spleen, thymus, mesenteric lymph nodes, pancreas, and kidney (Fig. 1A). C57BL/6-Tg(LTab)1223 mice (henceforth termed AlbLT $\alpha\beta$  mice) were identified as the highest expressors (Fig. 1B) and were selected for further experiments.

Livers from 4- to 6-month-old AlbLT $\alpha\beta$  mice displayed highly organized aggregates of B220<sup>+</sup> B lymphocytes; CD3<sup>+</sup>, CD4<sup>+</sup>, and CD8<sup>+</sup> T cells; FDC-M1<sup>+</sup> and CD35<sup>+</sup> networks; MOMA-1<sup>+</sup> marginal zone-like festoons; CD68<sup>+</sup> tingible body macrophages; IgD<sup>+</sup> and IgG1<sup>+</sup> lymphocytes; ERTR9<sup>+</sup> cells; and NLDC-145<sup>+</sup> DCs (Fig. 2) (fig. S1C). AlbLT $\alpha\beta$  sinusoids exhibited F4/80<sup>+</sup> Kupffer cell hyperproliferation and up-regulation of the adhesion molecules I-CAM and V-CAM (fig. S1C). Occasionally, PNA<sup>+</sup> clusters indicative of germinal center B cells were found (fig. S1C, arrowheads). None of the above features were found in livers of wild-type littermates (fig. S1C), nor could we detect abnormal histopathological features in AlbLT $\alpha\beta$  kidneys, spleens, and thymuses.

Transgenic mice expressing LT $\alpha$  under the control of the rat insulin promoter (RIP) in pancreatic  $\beta$  islet cells and renal proxi-

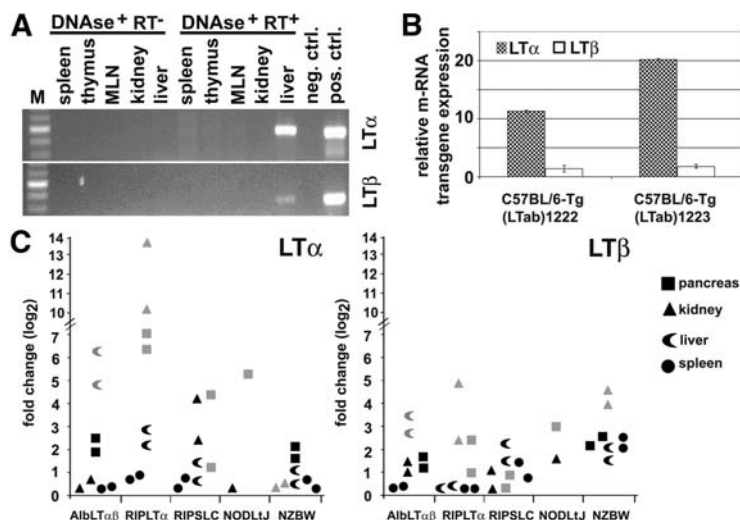


**Fig. 1.** Molecular and phenotypic characterization of AlbLT $\alpha\beta$  mice. (A) RT-PCR analysis, using primers 1 and 2 (450 bp) for transgenic LT $\alpha$  and primers 4 and 5 for transgenic LT $\beta$  (390 bp) (see fig. S1A), confirmed liver-specific transgene expression in AlbLT $\alpha\beta$  mice [negative control, master mix and H<sub>2</sub>O; positive control, transgenic plasmid DNA (10 ng)]. (B) Transgene-specific real-time RT-PCR analysis identifying C57BL/6-Tg(LTab)1222 as low LT $\alpha$  expressor and C57BL/6-Tg(LTab)1223 as high expressor. (C) Real-time RT-PCR identifying total LT $\alpha$  and LT $\beta$  expression in organs of mice with naturally occurring or transgenetically induced inflammatory and autoimmune diseases. Each value represents the fold change (log<sub>2</sub>) in individual organs relative to the average expression in two respective organs of control mice of the appropriate genotype. Each measurement was normalized against  $\beta$ -actin and expressed as fold change (log<sub>2</sub>) relative to the wild type. Gray and black symbols denote inflamed and noninflamed organs, respectively. LT $\alpha$  and/or LT $\beta$  were overexpressed not only in LT transgenic organs but also in inflamed organs of RIPSLC, NZBW, and NODLJ mice.

<sup>1</sup>Institute of Neuropathology, University Hospital of Zürich, CH-8091 Zürich, Switzerland. <sup>2</sup>Medical Research Council Prion Unit, Department of Neurodegenerative Diseases, Institute of Neurology, Queen Square, London WC1N 3BG, UK. <sup>3</sup>Department of Epidemiology and Public Health and Section of Immunobiology, Yale University School of Medicine, New Haven, CT 06520, USA.

\*These authors contributed equally to this work. †Present address: Institute of Neuropathology, Georg-August-Universität, D-37073 Göttingen, Germany. ‡To whom correspondence should be addressed. E-mail: adriano@pathol.unizh.ch

mal convoluted tubules (20–22) developed interstitial and capsular follicles in kidney and pancreatic islets with discrete B220<sup>+</sup> areas and CD35<sup>+</sup>/FDC-M1<sup>+</sup> networks (20, 21) (Fig. 2A). Renal and pancreatic inflammatory foci in RIPLT $\alpha$  and hepatic foci in AlbLT $\alpha\beta$  mice were essentially identical in their cellular composition and expressed various complement components (Fig. 2) (fig. S1D). The splenic and lymph nodal microarchitectures of RIPLT $\alpha$  ( $n = 5$ ), AlbLT $\alpha\beta$  ( $n = 3$ ), and wild-type mice ( $n = 3$ ) were indistinguishable upon immunostaining with an exhaustive panel of immunological markers (23).

We then studied mice expressing the secondary lymphoid organ chemokine (SLC), also known as TCA4/CCL21, under the control of the rat insulin promoter (22). These mice (henceforth termed RIPS LC) contain follicles in the pancreas with organized T and B cell zones, DCs, ER-TR7<sup>+</sup> and CD35<sup>+</sup> cells, and small FDC-M1<sup>+</sup> networks (Fig. 2) (23).

NZBxNZW-F<sub>1</sub> (henceforth termed NZBW) and NODLtJ mice are considered models for systemic lupus erythematosus and autoimmune diabetes, respectively. NZBW mice develop interstitial nephritis and glomerulonephritis with distinct B and T cell areas, small FDC-M1<sup>+</sup> clusters, DCs, small PNA<sup>+</sup> clusters, and IgG1<sup>+</sup> cells (Fig. 2) (fig. S1E). Infiltrates lacked MAcAdCam-1<sup>+</sup> expression but contained MOMA-1<sup>+</sup> cells (fig. S1E). Deposits of complement components C1q, C3, and C4 were identified within glomeruli of kidneys of NZBW mice, but not in parental NZW mice, which did not develop nephritis and were used as controls (Fig. 2) (fig.

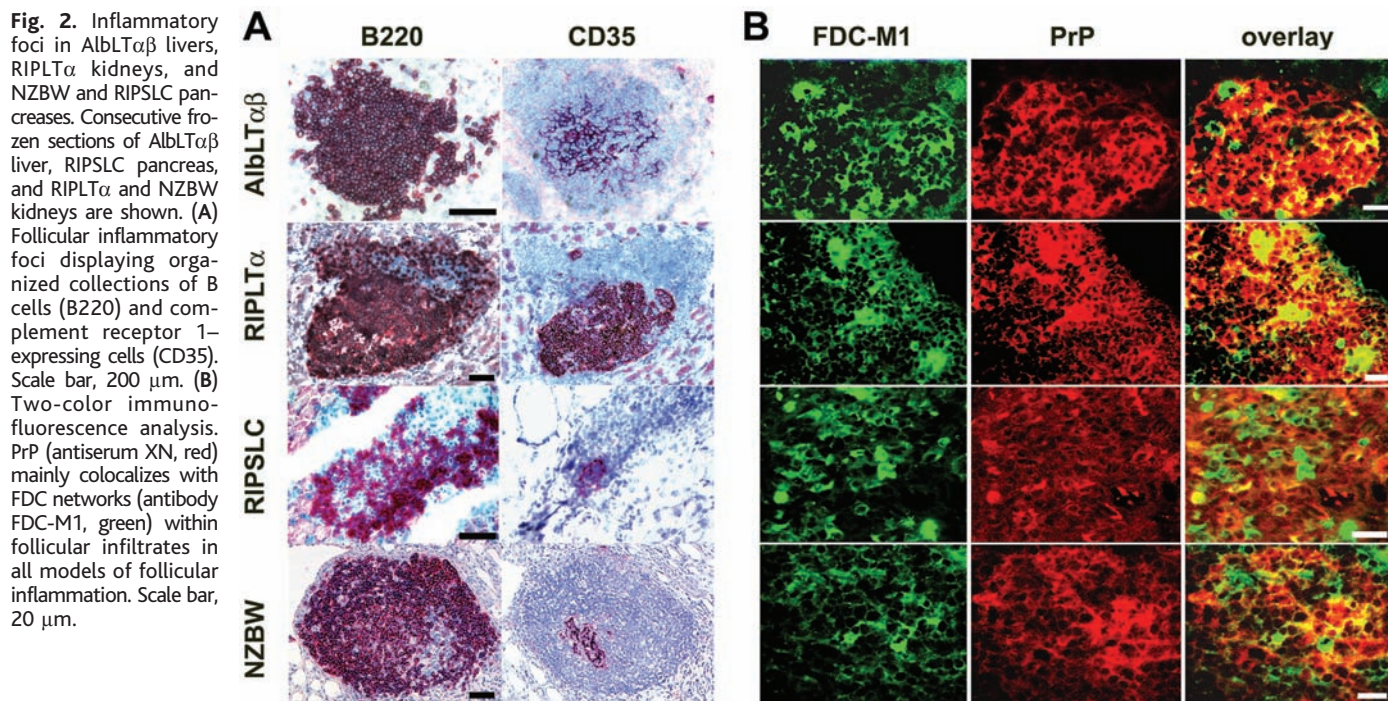
S1E) (23). NODLtJ mice develop spontaneous autoimmune insulinitis with lymphoid follicles similar to those developing in NZBW kidneys (24–26); NODB10.H2b mice, which do not develop insulinitis despite the presence of the NOD locus (27), were used as controls.

Real-time reverse transcription polymerase chain reaction (RT-PCR) analysis of LT $\alpha$  and LT $\beta$  expression in inflamed and appropriate control tissues revealed that 6- to 8-week-old AlbLT $\alpha\beta$  livers overexpressed LT $\alpha$  by a factor of ~45 and LT $\beta$  by a factor of 8 to 10 (Fig. 1C). LT expression declined in 8- to 12-month-old transgenic mice, in parallel with hepatocyte destruction. No other organs of AlbLT $\alpha\beta$  mice showed LT overexpression. RIPLT $\alpha$  mice overexpressed LT $\alpha$  and, to a lower extent, LT $\beta$  in kidney and pancreas, whereas RIPS LC mice had slightly up-regulated LT $\alpha$  expression in pancreas and kidney. LT $\alpha$  and LT $\beta$  were strongly up-regulated in NODLtJ pancreases, and LT $\beta$  was overexpressed in NZBW kidneys and pancreases. In summary, we detected LT up-regulation in every instance of chronic inflammation.

RIPLT $\alpha$ , RIPS LC, NZBW, NODLtJ, and isogenic or congenic control mice were inoculated with prions intraperitoneally [ $10^3$  times the median lethal dose (3 logLD<sub>50</sub>)] or intracerebrally (2.5 logLD<sub>50</sub>). RIPLT $\alpha$ , RIPS LC, and control mice showed similar incubation times and attack rates of disease (Fig. 3A), and the extent of terminal PrP<sup>Sc</sup> deposition was similar (fig. S2, A and B). The topography and intensity of spongiosis, gliosis, and PrP deposits were found by immunohistochemistry to be similar in the

brains of all terminally sick mice (23). Thus, chronic pancreatitis or nephritis did not influence susceptibility to intracerebrally or peripherally administered prions, nor did these conditions affect prion titers or neuroinvasion speed. Scrapie incubation times of NZBW and NODLtJ mice could not be determined because they exceeded their natural life span. The extent and morphology of inflammation in RIPLT $\alpha$  and RIPS LC kidneys and pancreases, as well as in AlbLT $\alpha\beta$  livers, were compared with age-matched mock-infected controls at several time points from 60 days post inoculation (dpi) to terminal disease. We did not detect any modulation of the inflammatory pathologies by prion infection, and intraperitoneal glucose tolerance was unaltered in prion-inoculated RIPLT $\alpha$  mice (fig. S2C).

We then sought to determine whether inflammation influences the distribution of prion infectivity during the preclinical phase of infection. AlbLT $\alpha\beta$ , RIPLT $\alpha$ , RIPS LC, NZBW, NZW (8 to 12 weeks old), NODLtJ, NODB10 (6 months old), and C57BL/6 mice were inoculated intraperitoneally with scrapie prions (5 logLD<sub>50</sub>) and killed at 60, 75, 90, or 100 dpi. Spleen homogenates were assayed for prion infectivity by mouse bioassay (MBA), consisting of intracerebral inoculation of *tga20* indicator mice (28) and comparison of scrapie incubation times to a calibration curve (29). All spleens displayed comparably high titers of prion infectivity per gram of tissue: 4.5 to 6 logLD<sub>50</sub>/g (wild type), 3.5 to 5 logLD<sub>50</sub>/g (RIPLT $\alpha$ ), 4.2 to 6.1 logLD<sub>50</sub>/g (AlbLT $\alpha\beta$ ), and 3.9 to 5.7 logLD<sub>50</sub>/g (RIPS LC). Attack rates of indicator mice were 100% at all time



points (Fig. 3B). Nephritis and pancreatitis did not affect splenic prion replication.

Prion loads of kidneys, pancreases, and livers from prion-infected presymptomatic mice were also determined by MBA (Fig. 3B). Titers were regarded as “borderline” if attack rates were <100%. At 60 dpi, wild-type pancreas and kidney homogenates lacked measurable infectivity, whereas RIPLT $\alpha$  kidney and pancreas titers ranged between borderline and 1.4 logLD<sub>50</sub>/g. At 75 dpi, RIPLT $\alpha$  pancreas and kidney titers were 3.3 and 4 logLD<sub>50</sub>/g, respectively, whereas wild-type pancreases and kidneys were noninfectious.

At 90 dpi, all RIPSCLC and RIPLT $\alpha$  pancreases and one RIPLT $\alpha$  kidney had prion titers approaching those of spleens (<3.7 logLD<sub>50</sub>/g in pancreas and <2.4 logLD<sub>50</sub>/g in kidney), whereas wild-type organs displayed undetectable or borderline infectivity (Fig. 3B). Infectivity of wild-type livers, kidneys, and AlBLT $\alpha\beta$  kidneys was borderline or below

detectability, whereas AlBLT $\alpha\beta$  livers had titers of 3.1 to 3.4 logLD<sub>50</sub>/g (Fig. 3B). NZBW kidneys were found to contain prion titers of 2.5 to 3.5 logLD<sub>50</sub>/g ( $n = 2$ ), whereas NZW kidneys were noninfectious (Fig. 3C).

We subjected organ extracts to scrapie cell assays in end point format (SCEPA) or to conventional scrapie cell assays (SCA), which allow for quantification of prion infectivity with sensitivity similar to MBAs (30). SCEPA and MBA results with RIPLT $\alpha$  kidney and pancreas homogenates (60 and 90 dpi) were almost completely congruent (fig. S2D and table S1). Wild-type kidneys and pancreases contained no detectable infectivity (<2.54 logLD<sub>50</sub>/g), whereas prion titers in the corresponding RIPLT $\alpha$  extracts were high (table S1). AlBLT $\alpha\beta$  liver prion titers (75 dpi) were >3.4 logLD<sub>50</sub>/g in all three liver homogenates, whereas no infectivity was detected in wild-type livers (<2.4 logLD<sub>50</sub>/g) (fig. S2E).

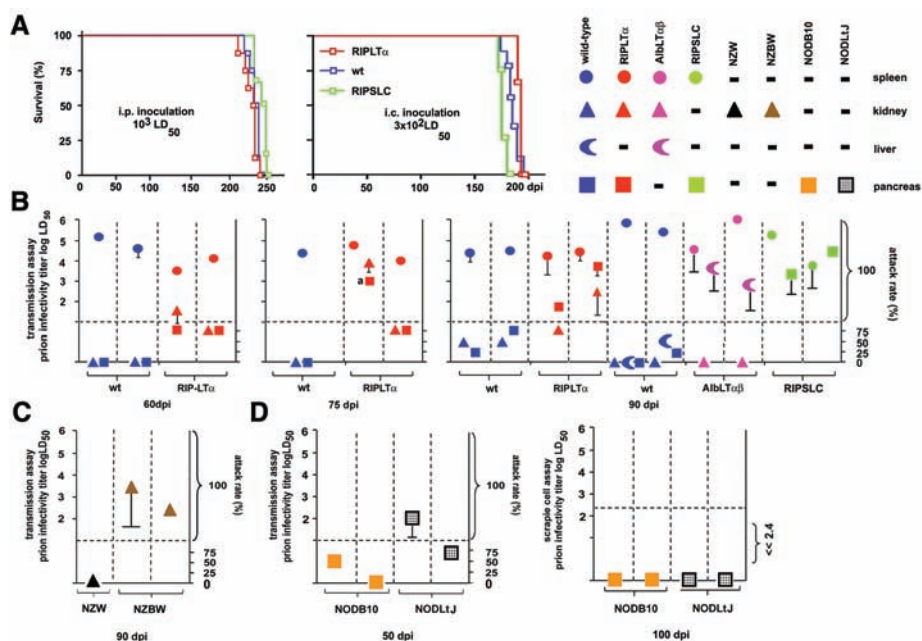


**Fig. 3.** The distribution of PrP<sup>Sc</sup> and prion infectivity is influenced by inflammatory conditions. (A) Survival plots of prion-infected RIPLT $\alpha$ , RIPSCLC, and wild-type (wt) mice, showing similar incubation times after intraperitoneal (i.p.; RIPLT $\alpha$ , 229 ± 10 days; wt, 234 ± 6 days; RIPSCLC, 243 ± 8 days) or intracerebral inoculation (i.c.; RIPLT $\alpha$ , 192 ± 2 days; wt, 185 ± 6 days; RIPSCLC, 174 ± 2 days). (B) Prion infectivity titers in spleens (circles), pancreases (squares), kidneys (triangles), and livers (crescents) of wild-type (wt) (blue), RIPLT $\alpha$  (red), AlBLT $\alpha\beta$  (pink), and RIPSCLC (green) mice were determined by transmission to indicator mice at 60, 75, and 90 dpi. Each column defined by vertical dashed lines represents one mouse. Data points below the dashed horizontal line indicate attack rates of <100% and were regarded as “borderline” infectivity. Error bars were drawn when standard deviation exceeded 0.75 log units. Except for one RIPLT $\alpha$  kidney that elicited an attack rate of 75%, RIPLT $\alpha$  kidneys and pancreases, RIPSCLC pancreases, and AlBLT $\alpha\beta$  livers led to an attack rate of 100% with high prion titers at 90 dpi. In contrast, wild-type kidneys, pancreases, and livers contained undetectable or at best borderline prion infectivity. (C) One of four *tga20* mice died shortly after inoculation from prion-unrelated causes. (D) Prion infectivity titers in kidneys (triangles) of NZW (black) and NZBW (brown) mice and in pancreases (squares) of NODB10 (orange) and NODLTJ (striped) mice were determined by transmission assay or SCEPA. At 90 dpi, NZBW kidneys harbored reasonably high infectivity titers, whereas NZW mice lacked prion infectivity (C). At 50 dpi, NODLTJ mice displayed borderline or moderate prion infectivity, whereas NODB10 mice showed no or borderline infectivity. At 100 dpi, NODLTJ mice were devoid of detectable prion infectivity, consistent with progressive islet elimination and consecutive regression of pancreatitis (D) (23).

We then administered scrapie prions (5 logLD<sub>50</sub>) intraperitoneally to 6-month-old NODLTJ mice and NODB10 mice. Pancreases of hyperglycemic NODLTJ mice contained prion titers of ≤2 logLD<sub>50</sub>/g at 50 dpi, whereas control NODB10 mice harbored no or borderline infectivity (Fig. 3D). All *tga20* mice ( $n = 7$ ) that had developed clinical scrapie upon exposure to pancreas homogenates (50 dpi) displayed spongiosis, gliosis, and PrP<sup>Sc</sup> in immunoblots (figs. S3 and S4), confirming transmission of scrapie infectivity. Similarly, all *tga20* mice that had developed clinical scrapie upon exposure to kidney, pancreas, and liver homogenates (AlBLT $\alpha\beta$ , RIPLT $\alpha$ , RIPSCLC, and NZBW) showed spongiosis, gliosis, and PrP<sup>Sc</sup> in immunoblots (figs. S3 and S4), confirming transmission of infectivity. However, at 100 dpi (~10 months of age), pancreatic infectivity was no longer detectable in either genotype, consistent with progressive islet elimination and consecutive regression of pancreatitis in NODLTJ mice (Fig. 3D) (23).

We then determined PrP<sup>Sc</sup> loads in organ extracts. Samples negative by conventional immunoblotting were reanalyzed after phosphotungstate (PTA) precipitation of PrP<sup>Sc</sup> (31), enhancing sensitivity (32). At 60, 75, and 90 dpi, PrP<sup>Sc</sup> was detectable in similar amounts in all spleens of each genotype, but not in livers, kidneys, or pancreases of wild-type mice (Fig. 4, A and B). At 60 dpi, PrP<sup>Sc</sup> was undetectable in livers, kidneys, or pancreases of any genotype. At 75 dpi, we found robust PrP<sup>Sc</sup> immunoreactivity in two of three AlBLT $\alpha\beta$  livers, but not in RIPLT $\alpha$  kidneys and pancreases (Fig. 4A). At 90 dpi, PrP<sup>Sc</sup> was readily detectable in all AlBLT $\alpha\beta$  livers (Fig. 4A), RIPLT $\alpha$  kidneys, and RIPLT $\alpha$  pancreases ( $n = 6$ , Fig. 4B). Possible PrP<sup>Sc</sup> traces were found in one wild-type kidney at 90 dpi (fig. S2F).

PTA-enhanced immunoblot analysis identified PrP<sup>Sc</sup> in NZBW ( $n = 2$ ) but not in NZW ( $n = 2$ ) kidneys (90 dpi) (Fig. 4C) (23). In contrast, PTA-enhanced immunoblotting failed to reveal PrP<sup>Sc</sup> in NODLTJ and NODB10 pancreases at all time points (50 and 100 dpi), consistent with the low infectivity titers of NODLTJ pancreases at 50 dpi (Fig. 3D).

By what mechanism does inflammation create novel prion reservoirs? PrP<sup>C</sup> is necessary for prion replication (4), hence its expression might be rate-limiting. We thus investigated PrP<sup>C</sup> expression in wild-type and RIPLT $\alpha$  kidneys and pancreases. Quantitative immunoblot analysis revealed ≤20% increase in total PrP<sup>C</sup> of RIPLT $\alpha$  kidneys, and no changes were seen in transgenic pancreases (fig. S1F). In contrast, immunohistochemical analysis revealed foci of high PrP expression in all analyzed AlBLT $\alpha\beta$  livers, RIPLT $\alpha$  kidneys and pancreases, RIPSCLC pancreases, NZBW kidneys, and NODLTJ pancreases (Fig. 2B), but not in

organs of the appropriate control mice. These foci mostly colocalized with FDC-M1<sup>+</sup> networks (Fig. 2B).

To characterize the topography of PrP<sup>Sc</sup> in inflamed prion-infected organs, we assayed (33) wild-type, RIPLT $\alpha$ , NZBW, and NZW kidneys as well as RIPSCLC pancreases by histoblotting. RIPLT $\alpha$  kidneys and pancreases (90 dpi) displayed PrP<sup>Sc</sup> deposits colocalizing with inflammatory infiltrates, whereas neither feature was found in scrapie-infected wild-type kidneys or pancreases (Fig. 4D). RIPSCLC pancreases and NZBW kidneys (90 dpi) also showed small PrP<sup>Sc</sup>-positive areas colocalizing with inflammatory infiltrates, whereas controls were devoid of PrP<sup>Sc</sup>-positive areas (23).

Inflammatory conditions cause immune cells to migrate into parenchymal sites of pathology. Some of these immune cells—including activated B lymphocytes—express LTs, which in turn trigger differentiation of FDCs. LT-triggered events, most likely including PrP<sup>C</sup> up-regulation in stromal FDC precursors, appear to confer prion replication competence to sites of inflammation. LT might thus represent a crucial link between inflammation and prion distribution. We tested this prediction by administering prions intraperitoneally to 6- to 8-month-old LT $\alpha^{-/-}$  and LT $\beta R^{-/-}$  mice, which suffer from spontaneous inflammatory pathologies (34), and to age-matched controls. Despite severe multifocal chronic lymphocytic hepatitis with disseminated PNA<sup>+</sup> clusters (fig. S5, A and B), livers

of prion-inoculated LT $\alpha^{-/-}$  and LT $\beta R^{-/-}$  mice were found to be consistently devoid of prion infectivity (fig. S5C) and PrP<sup>Sc</sup> (fig. S5D).

Our results indicate that chronic follicular inflammation, induced by a variety of causes, specifies prion tropism for otherwise prion-free organs. In most instances infectivity tended to rise with time, suggesting local prion replication. Organ-specific expression of one single proinflammatory cytokine (LT $\alpha$ ) or chemokine (SLC) sufficed to establish unexpected prion reservoirs, suggesting differentiation of ubiquitous stromal constituents into prion replication-competent cells. In several instances, prion concentration in individual inflamed organs approached that of spleen long before any clinical manifestation of scrapie. Inflamed nonlymphoid organs not only accumulated PrP<sup>Sc</sup> but also transmitted bona fide prion disease when inoculated into healthy recipient mice.

Knowledge of the distribution of prions within infected hosts is fundamental to consumer protection and prevention of iatrogenic accidents. On the basis of the failure to transmit bovine spongiform encephalopathy (BSE) infectivity from any tissue but central nervous system, intestinal, and lymphoid tissue (35), the risk to humans of contracting prion infection from other organs has been deemed small even in countries with endemic BSE. It may be important now to test whether superimposed viral, microbial, or autoimmune pathologies of farm animals trigger unexpected shifts in the organ tropism

of prions. Conversely, the lack of infectivity in “burned-out” postinflammatory pancreases suggests that anti-inflammatory regimens may abolish ectopic prion reservoirs.

References and Notes

1. H. Fraser, A. G. Dickinson, *Nature* **226**, 462 (1970).
2. S. B. Prusiner, *Science* **216**, 136 (1982).
3. G. Legname et al., *Science* **305**, 673 (2004).
4. H. R. Büeler et al., *Cell* **73**, 1339 (1993).
5. M. Gonzalez, F. Mackay, J. L. Browning, M. H. Kosco-Vilbois, R. J. Noelle, *J. Exp. Med.* **187**, 997 (1998).
6. T. Kitamoto, T. Muramoto, S. Mohri, K. Dohura, J. Tateishi, *J. Virol.* **65**, 6292 (1991).
7. K. L. Brown et al., *Nature Med.* **5**, 1308 (1999).
8. M. Prinz et al., *Nature* **425**, 957 (2003).
9. F. Montrasio et al., *Science* **288**, 1257 (2000).
10. N. A. Mabbott, G. McGovern, M. Jeffrey, M. E. Bruce, *J. Virol.* **76**, 5131 (2002).
11. M. Prinz et al., *Proc. Natl. Acad. Sci. U.S.A.* **99**, 919 (2002).
12. A. Aguzzi, *Nature Cell Biol.* **6**, 290 (2004).
13. S. Takemura et al., *J. Immunol.* **167**, 1072 (2001).
14. E. Kaiserling, *Lymphology* **34**, 22 (2001).
15. J. C. Hogg et al., *N. Engl. J. Med.* **350**, 2645 (2004).
16. W. Vernau, R. M. Jacobs, V. E. Valli, J. L. Heeney, *Vet. Pathol.* **34**, 222 (1997).
17. M. A. Klein et al., *Nature Med.* **7**, 488 (2001).
18. R. Magliozzi, S. Columba-Cabezas, B. Serafini, F. Aloisi, *J. Neuroimmunol.* **148**, 11 (2004).
19. See supporting data on Science Online.
20. D. E. Picarella, A. Kratz, C. B. Li, N. H. Ruddle, R. A. Flavell, *Proc. Natl. Acad. Sci. U.S.A.* **89**, 10036 (1992).
21. A. Kratz, A. Campos-Neto, M. S. Hanson, N. H. Ruddle, *J. Exp. Med.* **183**, 1461 (1996).
22. L. Fan, C. R. Reilly, Y. Luo, M. E. Dorf, D. Lo, *J. Immunol.* **164**, 3955 (2000).
23. M. Heikenwalder et al., data not shown.
24. A. Hanninen et al., *J. Clin. Invest.* **92**, 2509 (1993).
25. T. L. Delovitch, B. Singh, *Immunity* **7**, 727 (1997).
26. C. Faveeuw, M. C. Gagnerault, F. Lepault, *J. Immunol.* **152**, 5969 (1994).
27. C. P. Robinson et al., *Arthritis Rheum.* **41**, 150 (1998).
28. M. Fischer et al., *EMBO J.* **15**, 1255 (1996).
29. S. B. Prusiner et al., *Ann. Neurol.* **11**, 353 (1982).
30. P. C. Kohn, L. Stoltze, E. Flechsig, M. Enari, C. Weissmann, *Proc. Natl. Acad. Sci. U.S.A.* **100**, 11666 (2003).
31. J. Safar et al., *Nature Med.* **4**, 1157 (1998).
32. J. D. F. Wadsworth et al., *Lancet* **358**, 171 (2001).
33. A. Taraboulos et al., *Proc. Natl. Acad. Sci. U.S.A.* **89**, 7620 (1992).
34. A. Futterer, K. Mink, A. Luz, M. H. Kosco-Vilbois, K. Pfeffer, *Immunity* **9**, 59 (1998).
35. G. A. Wells et al., *Vet. Rec.* **142**, 103 (1998).
36. We thank S. Nedospasov and D. Kuprash for LT $\alpha/\beta$  cDNA; D. Lo for Ins-TCA4/SLC mice; C. Sigurdson, G. Miele, M. Zabel, F. Montrasio, and M. Le Hir for discussions; A. Gaspert and W. Jochum for histopathological advice; and B. Odermatt, R. Moos, and G. Bosshard for support with immunohistochemistry and SCA. Supported by grants from the Bundesamt für Bildung und Wissenschaft, the Swiss National Science Foundation, and the National Center of Competence in Research (NCCR) on Neural Plasticity and Repair (A.A.); by the foundation for research at the Medical Faculty, University of Zürich, a generous educational grant of the Catello family, and a grant of the Verein zur Förderung des Akademischen Nachwuchses (M.H.); by the Medical Research Council, UK (P.-C.K. and C.W.); and by NIH grant NCI R01 CA 16885 (N.H.R.).

Supporting Online Material

www.sciencemag.org/cgi/content/full/1106460/DC1  
 Materials and Methods  
 Figs. S1 to S5  
 Table S1  
 References

18 October 2004; accepted 6 December 2004  
 Published online 20 January 2005;  
 10.1126/science.1106460  
 Include this information when citing this paper.

**Fig. 4.** PrP<sup>Sc</sup> accumulates in inflamed organs of prion-infected mice. (A) Immunoblot analysis of liver homogenates after PTA precipitation at 75 dpi (upper blot) and 90 dpi (lower blot). PrP<sup>Sc</sup> was absent in all four individual wild-type livers, but clear PrP<sup>Sc</sup> signal was seen in four of five AlbLT $\alpha\beta$  livers. Control samples (ctrl.) included undigested healthy brain, proteinase K (PK)-digested healthy brain, and PK-digested terminally scrapie-sick brain. PTA, sodium phosphotungstate precipitation. (B) Immunoblot analysis showed strong PrP<sup>Sc</sup> signal in spleen, kidney, and pancreas of prion-infected RIPLT $\alpha$  mice (90 dpi), whereas PrP<sup>Sc</sup> was confined to spleens of wild-type mice. (C) Immunoblot of NZBW and NZW mice. PrP<sup>Sc</sup> was detected in kidneys of NZBW but not NZW mice. (D) Histoblot analysis of prion-infected kidneys. Capsular and subcapsular deposits of PrP<sup>Sc</sup> colocalize with follicular infiltrates in RIPLT $\alpha$  kidneys. Consecutive sections display colocalization of PrP<sup>Sc</sup> deposits with follicular infiltrates [hematoxylin and eosin (H&E) stain].

